Applied Surface Science 529 (2020) 147042

Contents lists available at ScienceDirect

Applied Surface Science

journal homepage: www.elsevier.com/locate/apsusc

Full Length Article

Cooling rate dependence of Ni-catalyzed transformation of amorphous carbon into graphene in rapid thermal processing: An experimental and reactive molecular dynamics study

Xiaowei Li[a,b,d,*], Hanchao Li[b], Kwang-Ryeol Lee[a], Aiying Wang[b,c,*]

[a] Computational Science Center, Korea Institute of Science and Technology, Seoul 136-791, PR China
[b] Key Laboratory of Marine Materials and Related Technologies, Zhejiang Key Laboratory of Marine Materials and Protective Technologies, Ningbo Institute of Materials Technology and Engineering, Chinese Academy of Sciences, Ningbo 315201, PR China
[c] Center of Materials Science and Optoelectronics Engineering, University of Chinese Academy of Sciences, Beijing 100049, PR China
[d] School of Materials and Physics, China University of Mining and Technology, Xuzhou 221116, PR China

ARTICLE INFO

Keywords:
Graphene
Amorphous carbon
Cooling rate
Rapid thermal process
Reactive molecular dynamics

ABSTRACT

Amorphous carbon with Ni as catalyst can be transformed into graphene on the dielectric substrate directly without the subsequent transfer process during rapid thermal processing (RTP). However, the effect of cooling rate on this transformation process is still not fully understood yet, leading to the controversy of underlying mechanism. Here, by the combined reactive molecular dynamics simulation with experimental approach, we investigated the evolution of RTP graphene structure and diffusion behavior of C atoms with cooling rates. Results demonstrated that for each case, there were no C atoms precipitated from C-Ni intermixing layer during the cooling process, which was different from the behavior observed in the Ni-catalyzed CVD growth process of graphene. This confirmed that the a-C-to-graphene transformation mechanism during the RTP process was dominated by the C diffusion and Ni-induced crystallization rather than the traditional dissolution/precipitation mechanism for graphene growth. Most importantly, it was also found that tailoring the cooling rate could achieve the regular arrangement of distorted structure in as-grown RTP graphene and thus promote the high-quality synthesis of graphene, which was confirmed by the experimental result.

1. Introduction

Graphene has been attracting ever-growing attention due to its fascinating performance such as high mechanical strength [1], optical transparency [2], width-tunable band gap [3], mobility of charge carriers [4], and thermal conductivity [5]. Since the discovery of the first isolated graphene prepared by mechanical exfoliation [6], many approaches to synthesize the graphene with large scale and high quality have been developed, including epitaxial growth [7], liquid-phase exfoliation [8], and chemical vapor deposition (CVD) [9]. However, the clean transfer of graphene from the metal growth substrate to a device-compatible substrate remains a big challenge, which is inevitably accompanied by the additional cost and the degradation of graphene quality, including wrinkles, cracks, and contamination [10–12].

Recent studies [13–16] reported that using the rapid thermal processing (RTP) method, a fast transfer-free synthesis of graphene structure on a dielectric substrate was successfully achieved by the solid-state transformation of amorphous carbon (a-C) in the presence of a catalytically active transition metal. This is strategically essential to directly grow the graphene on any possible dielectric substrate without the transfer process. However, previous studies mainly focused on characterizing the structural properties of graphene obtained in experiment [13–16], the fundamental insight into the a-C-to-graphene transformation and the dependence of RTP graphene quality on processing parameters from the atomic scale are not fully understood yet, which is essential to both the scientific understanding and practical implementation of a-C-to-graphene transformation approach. Especially, as well known that for the Ni-catalyzed CVD growth of graphene, the cooing rate plays a significant role in the thickness and quality of the graphene by controlling the segregation behaviors of C atoms from Ni catalyst [17–20]. But the influence of cooling rate on the a-C-to-graphene transformation, especially the corresponding structural evolution of as-grown graphene, diffusion behavior of C and Ni, and possible dissolution/precipitation behavior that exists in Ni-catalyzed CVD

* Corresponding authors at: Key Laboratory of Marine Materials and Related Technologies, Zhejiang Key Laboratory of Marine Materials and Protective Technologies, Ningbo Institute of Materials Technology and Engineering, Chinese Academy of Sciences, Ningbo 315201, PR China.
E-mail addresses: lixw0826@gmail.com (X. Li), aywang@nimte.ac.cn (A. Wang).

https://doi.org/10.1016/j.apsusc.2020.147042
Received 8 October 2019; Received in revised form 9 March 2020; Accepted 19 June 2020
Available online 27 June 2020

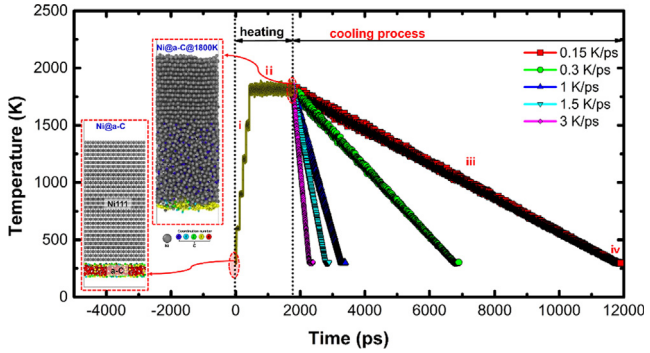

Fig. 1. Evolutions of temperature during the four-step process, including (i) a heating process from 300 to 1800 K, (ii) a diffusion process at 1800 K, (iii) a cooling process from 1800 to 300 K via different cooling rates, and (iv) final structural relaxation. The insets are the initial simulation model (Ni@a-C) and the structure with as-grown RTP graphene after diffusion at 1800 K for 1350 ps (Ni@a-C@1800 K).

growth of graphene, is still unclear, resulting in the controversy of underlying transformation mechanism [13–16].

In the present work, by the combined approach of reactive molecular dynamics (RMD) simulation with experiment, we selected Ni as catalyst and systematically explored the diffusion behaviors of C and Ni and the structural evolution of as-grown RTP graphene at different cooling rates. The results showed that during the cooling process, the a-C-to-graphene RTP method exhibited different dissolution/precipitation behaviors from the traditional Ni-catalyzed CVD technique, suggesting the difference in the grown mechanism of graphene. In addition, the appropriate selection of RTP cooling rate could effectively polish the structure of as-grown RTP graphene and thus facilitate the high-quality synthesis of graphene in the experiment.

2. Computational and experimental methods

2.1. Computational method

The inset of Fig. 1 showed the initial 3D model consisted of the bottom a-C and upper Ni111 layers (Ni@a-C) with the size of 30.672 × 26.06 × 128.5 $Å^3$, which contained 4320 Ni atoms and 872 C atoms. The a-C structure, obtained by ab initio MD simulation using the liquid-quenching method [21,22], had a density of 3.22 g/cm^3, an sp^3 fraction of 63.3 at.% and sp^2 fraction of 25.7 at.%. The average lattice mismatches between the Ni111 and a-C layers were 2.6% in the *x*-direction and 0.6% in the *y*-direction, respectively. A vacuum of 55 Å was employed in the direction perpendicular to the top Ni surface to avoid spurious interactions across the periodic boundaries, and the initial distance between the Ni and a-C layers was 3 Å.

All calculations were performed by the Large-scale Atomic/Molecular Massively Parallel Simulator (LAMMPS) code [23], and ReaxFF potential developed by Mueller *et al.* [24] was used to describe the interaction between the C and Ni atoms, which has been validated by additional RMD and ab-initio calculations, as shown in our previous study [25]. The time step was 0.25 fs, and the periodic boundary condition was employed along *x* and *y* directions. During the simulation process, there was no layer fixed to simulate the diffusion behavior of Ni and C atoms in the system [26]. As shown in Fig. 1, a four-step process was adopted: (i) a heating process from 300 to 1800 K using *NVT* ensemble with a Nose-Hoover thermostat [27] by stepwise heating strategy [22] to slowly overcome these energy barriers for structural transformation, (ii) a diffusion process at 1800 K for 1350 ps to obtain the structure with as-grown RTP graphene (named as Ni@a-C@1800 K, see the inset in Fig. 1) [25], (iii) a cooling process from 1800 to 300 K in the cooling rates of 0.15, 0.3, 1, 1.5, and 3 K/ps, respectively, to investigate the effect of different cooling rates on the RTP graphene quality, and (iv) final structural relaxation at 300 K for 125 ps.

2.2. Experimental method

In order to fabricate the Ni@a-C sample in experiment, the Si wafer with a 300 nm-thick thermally oxidized SiO_2 layer was used as substrate. Before the deposition process, the substrate was cleaned in acetone and ethanol, respectively, for 10 min. Then, it was placed in the vacuum chamber of home-made double bend filtered cathode vacuum arc (FCVA) equipment; when the chamber pressure was evacuated to 2.0×10^{-5} Torr, the a-C film (~2 nm) was deposited on the substrate. After that, the subsequent deposition of Ni film with a thickness of 80 nm was conducted by the magnetron sputtering approach.

For the deposited SiO_2/a-C/Ni sample, a Rapid Thermal Processor (MTI-OTF-1200X) was adopted to undertake the following RTP treatment. During the whole RTP process, the sample was first heated to 1073 K in the rate of 100 °C/min and then held the temperature for 10 min. After that, the sample was cooled to 300 K in the different rates of 100, 50, and 30 °C/min, respectively. Raman spectroscopy (Renishaw inVia Reflex) with 532 nm excitation wavelength and 5mW laser power incident was used to characterize the quality of graphene obtained from the RTP sample.

3. Results and discussion

Fig. 2 shows the final morphologies of Ni@a-C systems at the different cooling rates (0.15 ~ 3 K/ps) and the structure obtained after diffusion at 1800 K for 1350 ps is also given for comparison. It can be seen that after the cooling process, the whole system tends to be arranged orderly for each case, as will be described later. In particular, compared to the Ni@a-C@1800 K structure, the number of C atoms, which contributes to the formation of RTP graphene, decreases slightly, which are 406 for Ni@a-C@1800 K case, 390 for 3 K/ps, 379 for 1.5 K/ps, 363 for 1 K/ps, 318 for 0.3 K/ps, and 257 for 0.15 K/ps, respectively. This indicates that during the cooling process, there are no C atoms precipitated from C-Ni mixing region, consistent with that reported by Chen et al. [26]. However, this is against the popular Ni-catalyzed dissolution/precipitation mechanism for the graphene growth through CVD method [28,29].

Fig. 3 illustrates the profiles of C and Ni atomic fractions along the diffusion couple direction in the Ni@a-C systems. By comparison with the Ni@a-C@1800 K case, although a few number of C atoms further diffuse into Ni layer during the cooling process for each case, there is still a slight thickness reduction of diffusion zone (gray region in Fig. 3) observed except for the case with cooling rate of 0.15 K/ps, which attributes to the volume contraction induced by the drop in temperature. However, with cooling rate ranged from 3 to 0.15 K/ps, the thickness of diffusion zone increases slightly, which is consistent with the change of C-Ni plateau region (light blue regions in Fig. 3). In addition, the Ni/C ratio in the plateau region remains a constant of 5/1.

The mean square displacements (MSD) for C and Ni atoms in the system are calculated to evaluate the diffusion behavior of C and Ni atoms, as illustrated in Fig. 4. Note that during the cooling process, the MSD increases first and then decreases gradually for each case. When the cooling rate is 0.15 K/ps, the duration at the high temperature is much higher than other cases, so the increase of MSD for C atoms is more significant, resulting in more C atoms diffused into Ni layer. This is in consistence with the results in Figs. 2 and 3. However, with further cooling the system, the slow decreasing slope for MSD-time curve is observed as compared to those at 0.3, 1, 1.5, and 3 K/ps. This suggests that a high cooling rate is accompanied by the high diffusion coefficient to the contrary direction, attributing to the difference in the thermal gradient across the Ni layer [14]. The MSD for Ni atoms gives the similar behavior to that for C atoms, but the diffusion coefficient of Ni is much smaller than that of C for each case, which agrees well with Chen's report [26].

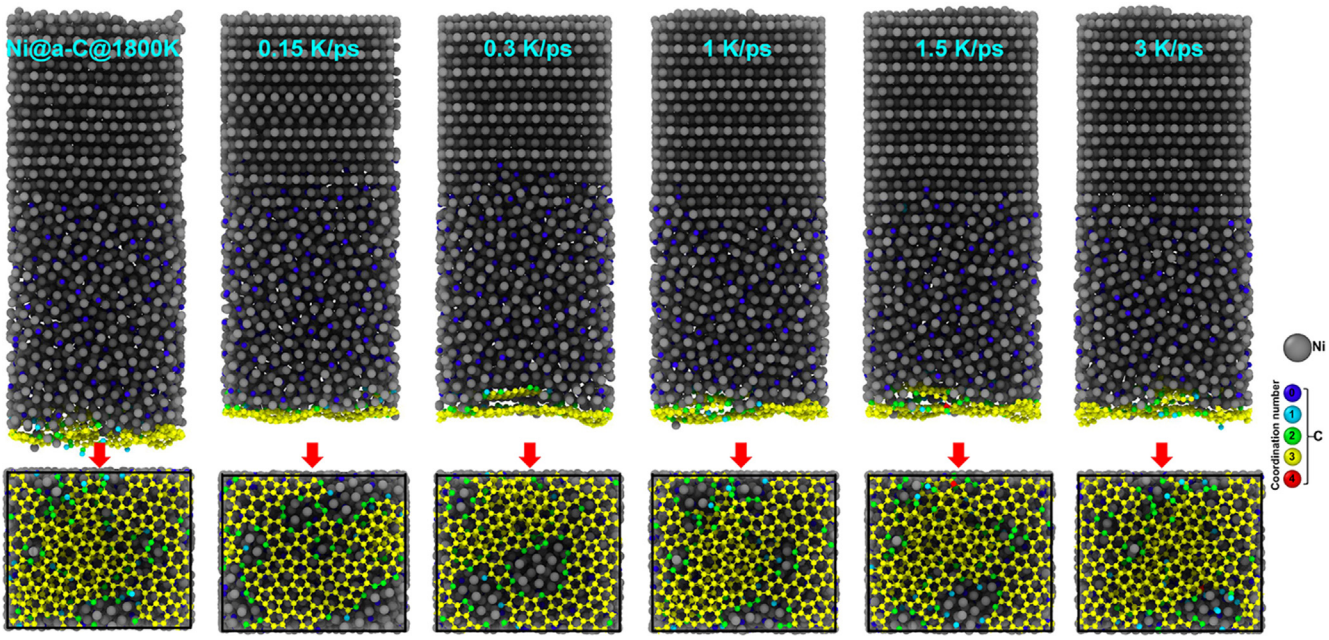

Fig. 2. Final morphologies of Ni@a-C systems at the different cooling rates (0.15 ~ 3 K/ps). The case after diffusion at 1800 K for 1350 ps (Ni@a-C@1800 K) is also given for comparison.

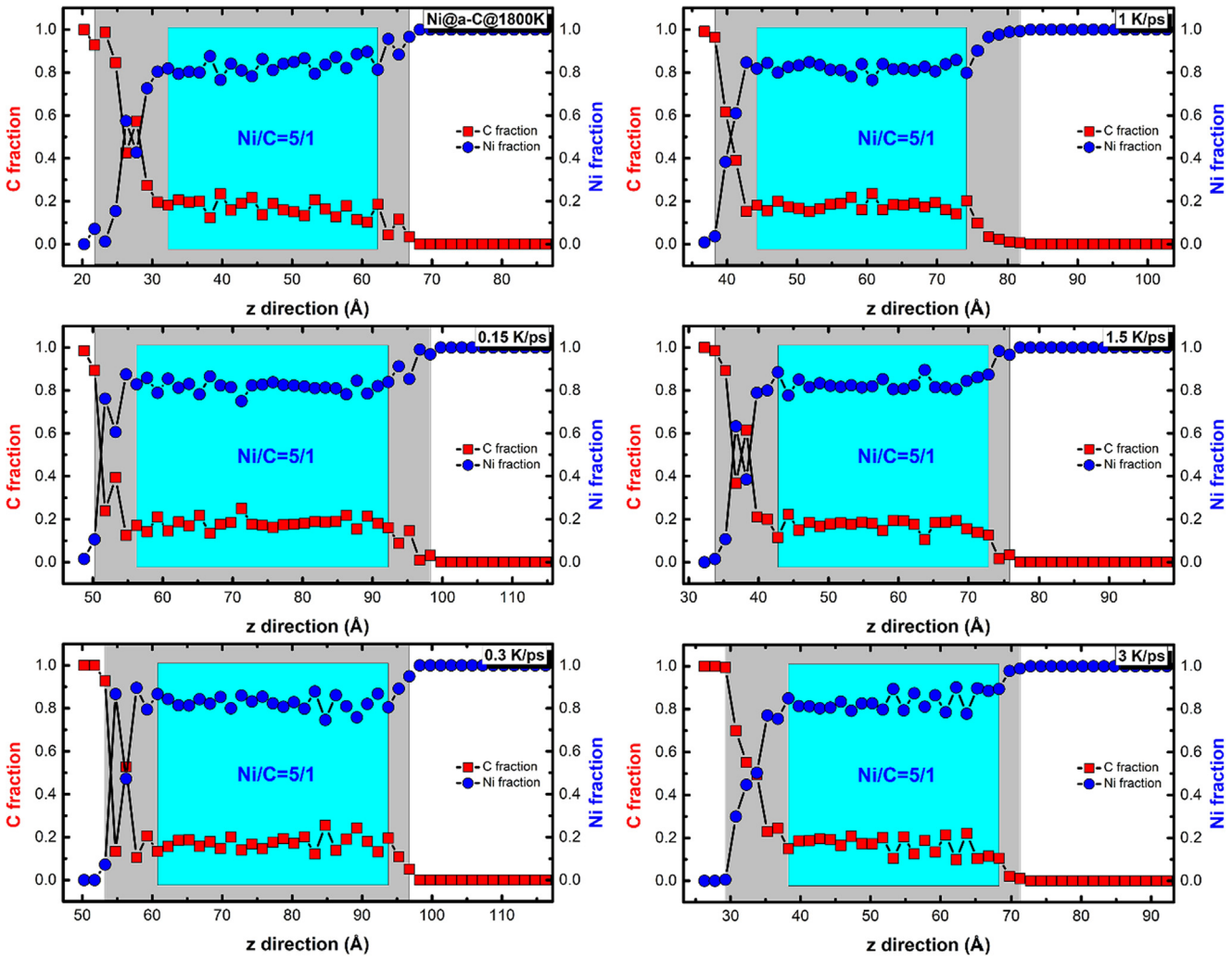

Fig. 3. Profiles of C and Ni atomic fractions along the diffusion couple direction in the Ni@a-C systems at the different cooling rates (0.15 ~ 3 K/ps). The result after diffusion at 1800 K for 1350 ps (Ni@a-C@1800 K) is also given for comparison.

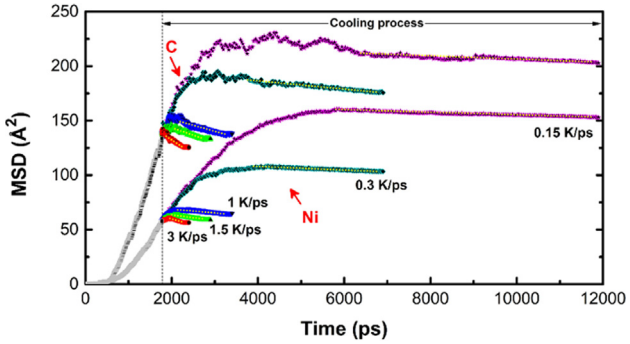

Fig. 4. MSD with diffusion time in the Ni@a-C systems at the different cooling rates (0.15 ~ 3 K/ps).

Furthermore, for each case, the Ni@a-C system can be divided into three main regions, including RTP graphene, C-Ni plateau, and top Ni regions. Fig. 5 gives the corresponding radial distribution function (RDF) spectrum for each region. In the Ni@a-C@1800 K structure (before the cooling process), the C-Ni plateau region shows a viscous liquid-like character [26], and the Ni region is also melted partially. Nevertheless, compared to the Ni@a-C@1800 K case, after the cooling process for each case, the peak intensity of RDF for RTP graphene increases and the peak intensities for C-Ni and Ni-Ni interactions in RDF spectra of C-Ni plateau also enhance significantly. Especially, the top Ni region restores to the obvious crystallized character from the liquid state. Hence, the RDF spectra clearly reveal the trend of regular distribution for Ni and C atoms in the system after the cooling process. In addition, with the cooling rate changed from 3 to 0.15 K/ps, the differences in the peak intensity and position of RDF spectra cannot be distinguished clearly.

In order to further explore the effect of different cooling rates on the a-C-to-graphene transformation, the bond structures of RTP graphene generated at different cooling rates are systematically analyzed. Fig. 6 shows the morphology of RTP graphene obtained after the cooling process for each case, in which the Ni and C atoms diffused into Ni layers are neglected for view. For comparison, the Ni@a-C@1800 K case is also considered. It can be seen that compared to the Ni@a-C@1800 K structure, the RTP graphene tends to be flat and ordered; in addition, with decreasing the cooling rate from 3 to 0.15 K/ps, there is an obvious reduction in the RTP graphene layers following the decreased number of C atoms and enlarged size of pore defects, attributing to the different diffusion behavior of C into Ni layer during the cooling process, as confirmed by the MSD in Fig. 4.

In the RTP graphene obtained at different cooling rates, the fraction

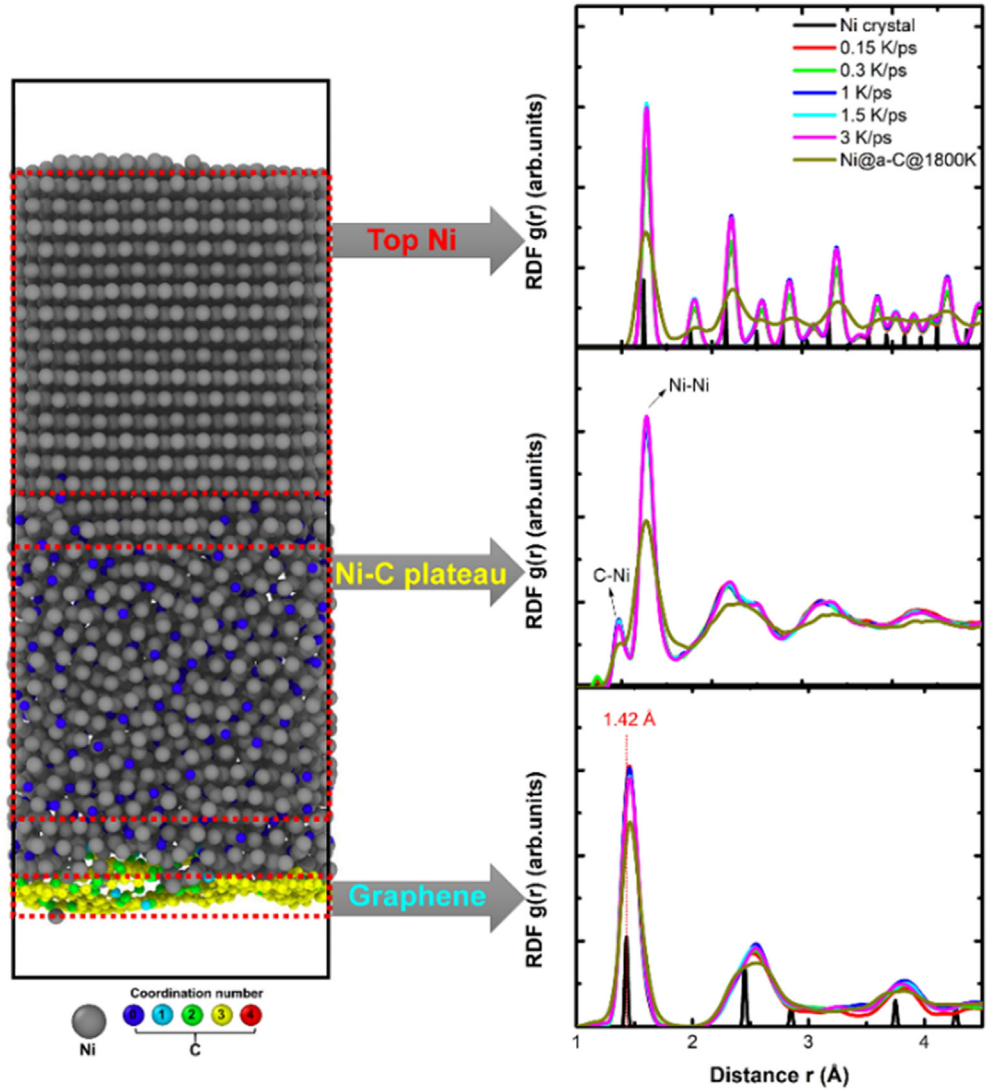

Fig. 5. RDF spectra for RTP graphene, C-Ni plateau, and top Ni regions in the Ni@a-C systems cooled at different rates. The results after diffusion at 1800 K for 1350 ps (Ni@a-C@1800 K) are also given for comparison.

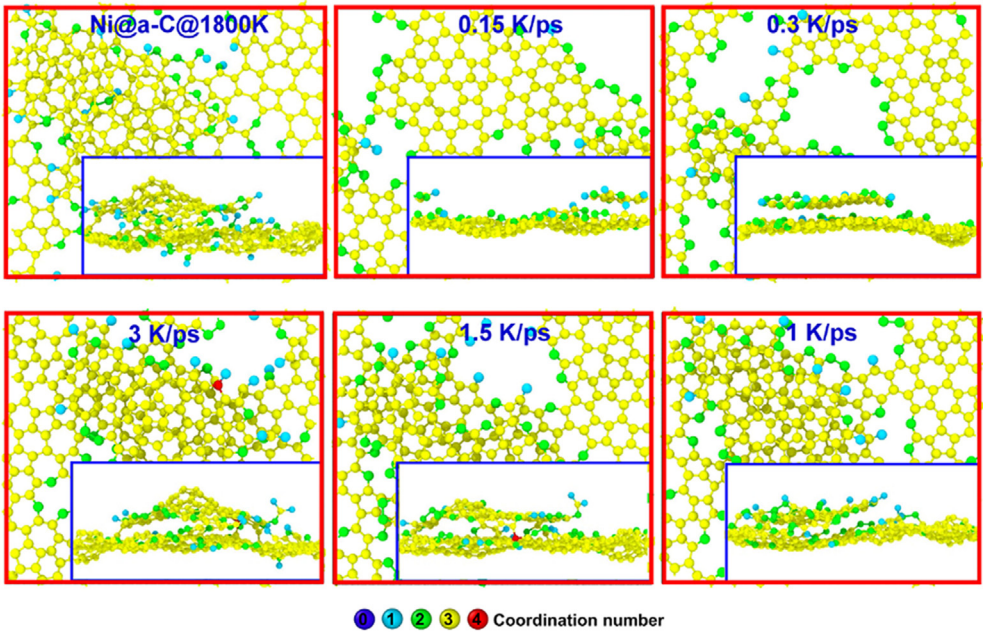

Fig. 6. Top and side views of RTP graphene morphologies obtained at different cooling rates, in which the Ni and C atoms diffused into Ni layers are neglected for view. The Ni@a-C@1800 K case is also given for comparison.

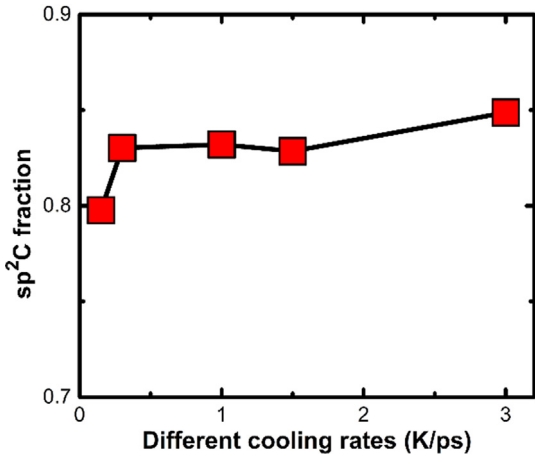

Fig. 7. Fraction of sp^2C hybridized structure in the RTP graphene obtained at different cooling rates. The Ni@a-C@1800 K case is also given for comparison.

of sp^2C hybridized structure is analyzed, as illustrated in Fig. 7. First, with the cooling rate decreased from 3 to 0.15 K/ps, the drop of sp^2C fraction is observed, suggesting the presence of graphitic dissolution into Ni layer during the cooling process [25]. This originates from the continuous diffusion of C into Ni layer at the initial cooling stage which is still located at the high temperature, as shown in Fig. 4. However, the change of sp^2C fraction with cooling rate in Fig. 7 displays three different stages, including the slow decreasing stage (3 ~ 1.5 K/ps), the stable stage (1.5 ~ 0.3 K/ps), and the fast decreasing stage (0.3 ~ 0.15 K/ps). This behavior not only highlights the role of cooling rate in the synthesis and layer modulation of RTP graphene transformed from a-C, but also indicates that too slow cooling rate, such as 0.15 K/ps, is not favorable to the generation of RTP graphene, while the cooling rate should be the one at which the as-grown RTP graphene can be polished effectively without scarifying the sp^2C fraction seriously, such as 1.5 ~ 0.3 K/ps in the present work. Therefore, in the following study, the comparative analysis of RTP graphene structures only focuses on the cooling rates ranged from 1.5 to 1 and 0.3 K/ps.

Fig. 8 gives the change of both the bond angle and length

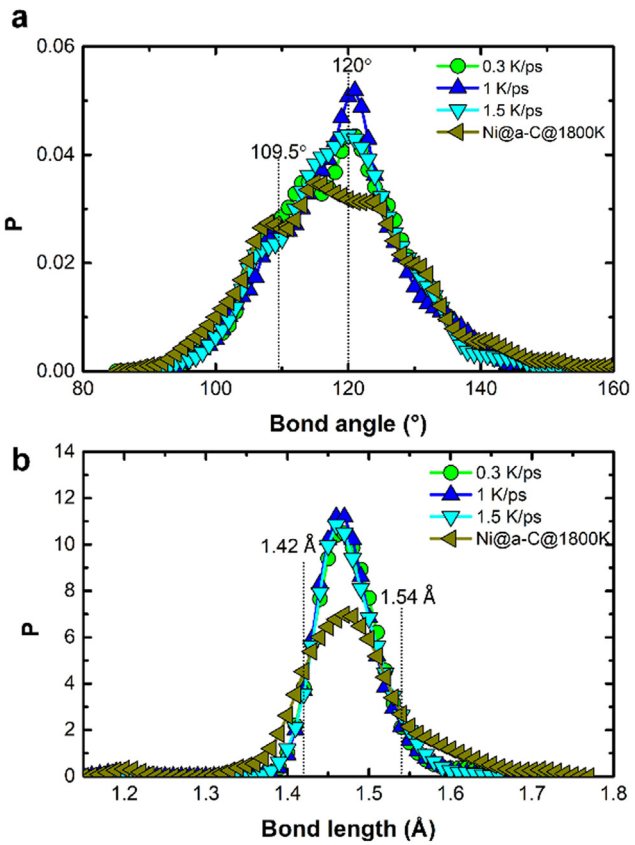

Fig. 8. (a) Bond angle and (b) length distributions of RTP graphene obtained at different cooling rates (1.5 ~ 0.3 K/ps). The result of Ni@a-C@1800 K is also given for comparison.

distributions of RTP graphene with cooling rate. When the cooling rate decreases from 1.5 to 0.3 K/ps, there is no change in the peak position of the bond angle distribution (Fig. 8a), but the peak intensity enhances first and then decreases, which is similar to that of the bond length distribution (Fig. 8b). So combined with the bond length and angle

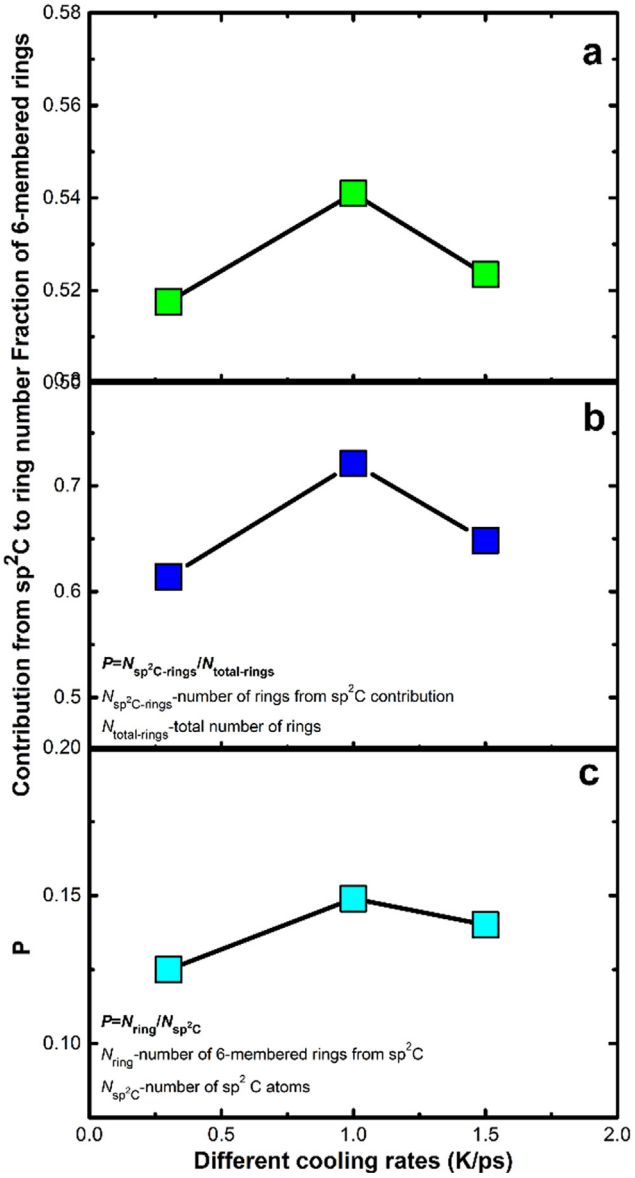

Fig. 9. (a) Fractions of 6-membered rings; (b) Proportion of the number of rings (5, 6, and 7-membered rings) contributed by sp^2C to the total number of rings; (c) Probability to form rings per sp^2C atom. The results of Ni@a-C@1800 K is also given for comparison.

distributions, the changes in peak width and intensity not only further confirm the regular arrangement of RTP graphene structure during the cooling process by comparison with the Ni@a-C@1800 K case, but also imply the structural optimization induced by the cooling rate. When the cooling rate is 1 K/ps, the maximal peak intensities are achieved, suggesting the best quality of RTP graphene.

By further analyzing the structure of rings in the obtained RTP graphene, Fig. 9a demonstrates that the fraction of 6-membered rings with cooling rate changed from 1.5 to 0.3 K/ps increases first and then decreases following the contrary change of both the 5- and 7-membered rings. Moreover, the proportion of the number of rings (5, 6, and 7-membered rings) contributed by sp^2C to the total number of rings and the probability to form rings per sp^2C atom are also evaluated (Fig. 9b and 9c), which all have the highest values at the cooling rate of 1 K/ps than other two cases. Therefore, the abovementioned structural analysis of RTP graphene clearly indicates that when the cooling rate is 1 K/ps, the RTP graphene has a high-quality crystalline structure.

Therefore, due to the difference in the formation mechanism of graphene between the a-C-transformed RTP approach and the CVD method, the cooling rate plays different roles in the growing process of graphene. For the a-C-to-graphene transformation via RTP, fast cooling rate prevents both the defective optimization and the structural regulation of as-grown graphene (Figs. 6, 8, and 9), which is different from Koh's report [30]. However, slow cooling rate promotes the excess dissolution of a large amount of graphitic structures (Fig. 7), accompanied by the reduction of graphene layers and the size enlargement of intrinsic pore defects (Fig. 6), which is contrary to the cases in the CVD growth of graphene reported by Mafra [17] and Seah [18]. The medium cooling rate, such as 1 K/ps in the present RMD simulation, facilitates the formation of graphene with high quality and ordered structure. This is also confirmed by the following Raman analysis of the samples synthesized in experiment after RTP treatment.

Fig. 10a illustrates the Raman spectra of the samples cooled at different rates in experiment. For each case, the spectrum is composed of three peaks, including D peak located at 1350 cm^{-1}, G peak located 1580 cm^{-1}, and 2D peak located 2700 cm^{-1}, respectively [30]. The fitting results of Raman spectra, including the I_D/I_G and I_{2D}/I_G ratios, are given in Fig. 10b. Xiong et al. [13] reported that an I_{2D}/I_G ratio located at between 0.8 and 1.4 normally corresponded to the formation of bilayer graphene, while the monolayer or few-layer graphene could be identified with an I_{2D}/I_G ratio of $>$ 1.4 or $<$ 0.8, respectively. When the cooling rate is 100 °C/min, I_{2D}/I_G ratio is about 0.43, corresponding to the three-layer graphene [30], but there is no enough time to crystalize or optimize the structure of as-grown graphene, resulting in the existence of many defects as confirmed by the high I_D/I_G ratio of 1.06 in Fig. 10. For the sample cooled at the rate of 50 °C/min, the formation of bilayer graphene with relative-high quality crystalline structure is suggested by the high I_{2D}/I_G ratio of 1.11 and the significant reduced I_D/I_G ratio of 0.46. However, with further decreasing the cooling rate to 30 °C/min from 50 °C/min, bilayer graphene is also achieved, but the increased I_D/I_G ratio (0.51) is related with the excess dissolution of the graphitic structure at the high temperature, breaking the uniformity and integrity of graphene structure. This change of microstructure of RTP graphene with cooling rate is also proved by the Raman mapping images with size of 10 μm × 10 μm, as illustrated in Fig. 10c and d. In addition, the presence of obvious D peak in Raman spectra (Fig. 10a) indicates the insufficient quality of the graphene structures obtained in experiment, but it is enough to disclose the key information about the effect of cooling rate on the formation of RTP graphene.

Especially, it should be mentioned that due to the limitation of short RMD simulation time and the differences in size and structure of Ni@a-C sample between the simulation and experiment, it is unrealistic to employ the same cooling rate to both cases, leading to the quantitative deviation of cooling rate value. But most importantly, the fundamental understanding about the dependence of a-C-to-graphene transformation on cooling rates, which is conveyed by the experiment result, is in consistence with that obtained by RMD simulation. This is requisite to the high quality synthesis of a-C-transformed graphene using RTP approach.

4. Conclusions

In conclusions, we performed a combined RMD simulation and experimental approach to study the dependence of diffusion behavior and graphene structure on the cooling rate during the a-C-to-graphene transformation process using the RTP method. Our simulation result revealed that during the cooling process, the system tended to be arranged orderly, but there were no C atoms precipitated from the C-Ni intermixing region, which subverted the dissolution/precipitation mechanism typically involved in Ni-catalyzed CVD growth of graphene. The difference in the formation mechanism of graphene between the a-C-transformed RTP approach and the CVD method brought the different roles of cooling rate in the growing process of graphene. With

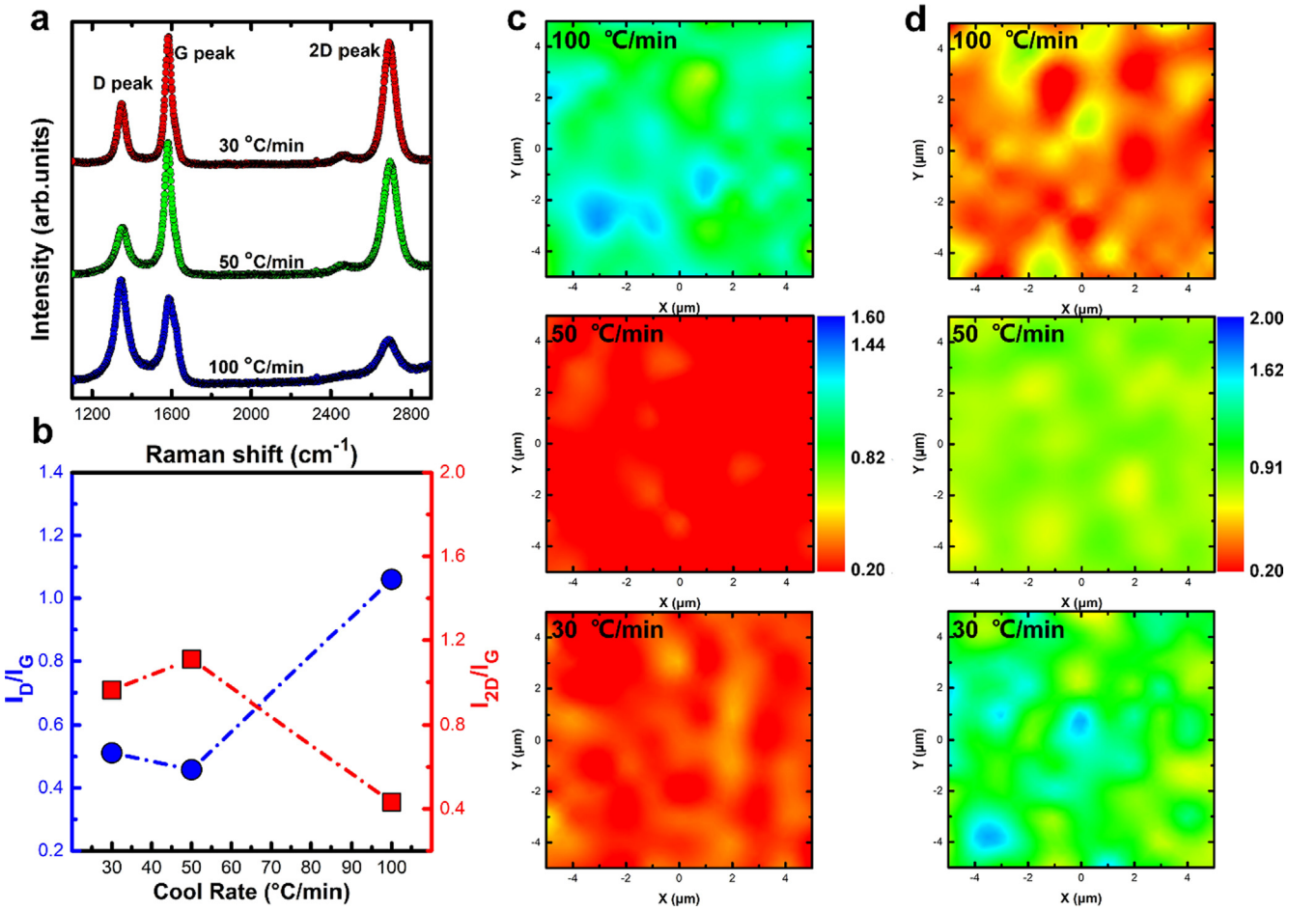

Fig. 10. Experimental results including (a) Raman spectra, (b) fitting results including the change of I_D/I_G and I_{2D}/I_G ratios, and corresponding mapping images of (c) I_D/I_G ratio and (d) I_{2D}/I_G ratio with cooling rate.

decreasing the cooling rate from 3 to 0.15 K/ps, the diffusion coefficient of C atoms increased first and then decreased, resulting in more C atoms diffused into Ni layer from as-grown graphene and the drop of sp^2C fraction of RTP graphene. Bond structure analysis revealed that compared to the cases at fast and slow cooling rates, the medium cooling rate facilitated the as-grown graphene to relax the distorted structure, tailor the bond angle, bond length, and ring fractions without the excess dissolution of graphitic structure, thus leading to the improvement of graphene in quality, which agreed with the experimental result qualitatively. The present study not only discloses the insight into a-C-to-graphene transformation during the cooling process, but also offers guidance for the selection of key processing parameters to fabricate the graphene structure with high quality.

CRediT authorship contribution statement

Xiaowei Li: Conceptualization, Data curation, Formal analysis, Methodology, Software, Validation, Investigation, Writing - original draft, Writing - review & editing, Funding acquisition. **Hanchao Li:** Data curation, Formal analysis, Methodology, Validation, Investigation. **Kwang-Ryeol Lee:** Conceptualization, Resources, Writing - review & editing, Funding acquisition. **Aiying Wang:** Conceptualization, Methodology, Resources, Investigation, Writing - review & editing, Supervision, Funding acquisition.

Declaration of Competing Interest

The authors declare that they have no known competing financial interests or personal relationships that could have appeared to influence the work reported in this paper.

Acknowledgments

This research was supported by the Korea Research Fellowship Program funded by the Ministry of Science and ICT through the National Research Foundation of Korea (2017H1D3A1A01055070), the Nano Materials Research Program through the Ministry of Science and IT Technology (NRF-2016M3A7B4025402), the National Natural Science Foundation of China (51772307), the A-class pilot of the Chinese Academy of Sciences (XDA22010303), and the Ningbo Science and Technology Innovation Project (2018B10014).

References

[1] X. Xue, Q. Yin, H. Jia, X. Zhang, Y. Wen, Q. Ji, Z. Xu, Enhancing mechanical and thermal properties of styrene-butadiene rubber/carboxylated acrylonitrile butadiene blend by the usage of graphene oxide with diverse oxidation degrees, Appl. Surf. Sci. 423 (2017) 584–591.
[2] H. Sun, D. Chen, C. Ye, X. Li, D. Dai, Q. Yuan, K.W.A. Chee, P. Zhao, N. Jiang, C.T. Lin, Large-area self-assembled reduced graphene oxide/electrochemically exfoliated graphene hybrid films for transparent electrothermal heaters, Appl. Surf. Sci. 435 (2018) 809–814.
[3] J. Yu, M. Zhang, J. He, C. Zhang, W. Cui, N. Wang, C. Huang, Tunable Fermi level of graphene modified by azobenzene molecules, Appl. Surf. Coat. 463 (2019) 900–906.
[4] H. Sun, X. Li, Y. Li, G. Chen, Z. Liu, F.E. Alam, D. Dai, L. Li, L. Tao, J.B. Xu, Y. Fang, X. Li, P. Zhao, N. Jiang, D. Chen, C.T. Lin, High-quality monolithic graphene films via laterally stitched growth and structural repair of isolated flakes for transparent electronics, Chem. Mater. 29 (2017) 7808–7815.
[5] B.S. Lee, Thermal conductivity and scattering models for graphene: From intrinsic

scattering of pristine graphene to strong extrinsic scattering of functionalized graphene, Appl. Surf. Sci. 497 (2019) 143739.
[6] K.S. Novoselov, A.K. Geim, S.V. Morozov, D. Jiang, Y. Zhang, S.V. Dubonos, I.V. Grigorieva, A.A. Firsov, Electric field effect in atomically thin carbon films, Science 306 (2004) 666–669.
[7] M. Jugovac, F. Genuzio, E.G. Lazo, N. Stojić, G. Zamborlini, V. Feyer, T.O. Menteş, A. Locatelli, C.M. Schneider, Role of carbon dissolution and recondensation in graphene epitaxial alignment on cobalt, Carbon 152 (2019) 489–496.
[8] G. Tubon Usca, J. Hernandez-Ambato, C. Pace, L.S. Caputi, A. Tavolaro, Liquid-phase exfoliated graphene self-assembled films: Low-frequency noise and thermal-electric characterization, Appl. Surf. Sci. 380 (2016) 268–273.
[9] Q. Liu, C. Yu, Z. He, G. Gu, J. Wang, C. Zhou, J. Guo, X. Gao, Z. Feng, Chemical vapor deposition graphene of high mobility by gradient growth method on an 4H-SiC(0001) substrate, Appl. Surf. Sci. 454 (2018) 68–73.
[10] G. Lupina, J. Kitzmann, I. Costina, M. Lukosius, C. Wenger, A. Wolff, S. Vaziri, M. Östling, I. Pasternak, A. Krajewska, W. Strupinski, S. Kataria, A. Gahoi, M.C. Lemme, G. Ruhl, G. Zoth, O. Luxenhofer, W. Mehr, Residual metallic contamination of transferred chemical vapor deposited graphene, ACS Nano 9 (2015) 4776–4785.
[11] X. Liang, B.A. Sperling, I. Calizo, G. Cheng, C.A. Hacker, Q. Zhang, Y. Obeng, K. Yang, H. Peng, Q. Li, X. Zhu, H. Yuan, A.R.H. Walker, Z. Liu, L. Peng, C.A. Richter, Toward clean and crackless transfer of graphene, ACS Nano 5 (2011) 9144–9153.
[12] X.D. Chen, Z.B. Liu, C.Y. Zheng, F. Xing, X.Q. Yan, Y. Chen, J.G. Tian, High-quality and efficient transfer of large-area graphene films onto different substrates, Carbon 56 (2013) 271–278.
[13] W. Xiong, Y.S. Zhou, L.J. Jiang, A. Sarkar, M. Mahjouri-Samani, Z.Q. Xie, Y. Gao, N.J. Ianno, L. Jiang, Y.F. Lu, Single-step formation of graphene on dielectric surfaces, Adv. Mater. 25 (2013) 630–634.
[14] Z. Wu, Y. Guo, Y. Guo, R. Huang, S. Xu, J. Song, H. Lu, Z. Lin, Y. Han, H. Li, T. Han, J. Lin, Y. Wu, G. Long, Y. Cai, C. Cheng, D. Su, J. Robertson, N. Wang, A fast transfer-free synthesis of high-quality monolayer graphene on insulating substrates by a simple rapid thermal treatment, Nanoscale 8 (2016) 2594–2600.
[15] M. Zheng, K. Takei, B. Hsia, H. Fang, X. Zhang, N. Ferralis, H. Ko, Y.L. Chueh, Y. Zhang, R. Maboudian, A. Javey, Metal-catalyzed crystallization of amorphous carbon to graphene, Appl. Phys. Lett. 96 (2010) 063110.
[16] J.A. Rodríguez-Manzo, C. Pham-Huu, F. Banhart, Graphene growth by a metal-catalyzed solid-state transformation of amorphous carbon, ACS Nano 5 (2011) 1529–1534.
[17] D.L. Mafra, J.A. Olmos-Asar, F.R. Negreiros, A. Reina, K.K. Kim, M.S. Dresselhaus, J. Kong, G.J. Mankey, P.T. Araujo, Ambient-pressure CVD of graphene on low-index Ni surfaces using methane: a combined experimental and first-principles study, Phys. Rev. Mater. 2 (2018) 073404.
[18] C.M. Seah, B. Vigolo, S.P. Chai, S. Ichikawa, J. Gleize, F.L. Normand, F. Aweke, A.R. Mohamed, Sequential synthesis of free-standing high quality bilayer graphene from recycled nickel foil, Carbon 96 (2016) 268–275.
[19] A. Reina, S. Thiele, X. Jia, S. Bhaviripudi, M.S. Dresselhaus, J.A. Schaefer, J. Kong, Growth of large-area single- and bilayer graphene by controlled carbon precipitation on polycrystalline Ni surfaces, Nano Res. 2 (2009) 509–516.
[20] Q. Yu, J. Lian, S. Siriponglert, H. Li, Y.P. Chen, S.S. Pei, Graphene segregated on Ni surfaces and transferred to insulators, Phys. Rev. Lett. 93 (2008) 113103.
[21] X. Li, P. Guo, L. Sun, A. Wang, P. Ke, Ab initio investigation on Cu/Cr codoped amorphous carbon nanocomposite films with giant residual stress reduction, ACS Appl. Mater. Interfaces 7 (2015) 27878–27884.
[22] X. Li, L. Li, D. Zhang, A. Wang, Ab initio study of interfacial structure transformation of amorphous carbon catalyzed by Ti, Cr, and W transition layers, ACS Appl. Mater. Interfaces 9 (2017) 41116–41119.
[23] S. Plimpton, Fast parallel algorithms for short-range molecular dynamics, J. Comp. Phys. 117 (1995) 1–19.
[24] J.E. Mueller, A.C.T. van Duin, W.A. Goddard III, Development and validation of ReaxFF reactive force field for hydrocarbon chemistry catalyzed by nickel, J. Phys. Chem. C 114 (2010) 4939–4949.
[25] X. Li, Y. Zhou, X. Xu, A. Wang, K.R. Lee, Role of the carbon source in the transformation of amorphous carbon to graphene during rapid thermal processing, Phys. Chem. Chem. Phys. 21 (2019) 9384–9390.
[26] S. Chen, W. Xiong, Y.S. Zhou, Y.F. Lu, X.C. Zeng, An ab initio study of the nickel-catalyzed transformation of amorphous carbon into graphene in rapid thermal processing, Nanoscale 8 (2016) 9746–9755.
[27] D.J. Evans, B.L. Holian, The nose-hoover thermostat, J. Chem. Phys. 83 (1985) 4069–4074.
[28] K.L. Saenger, J.C. Tsang, A.A. Bol, J.O. Chu, A. Grill, C. Lavoie, In situ X-ray diffraction study of graphitic carbon formed during heating and cooling of amorphous-C/Ni bilayers, Appl. Phys. Lett. 96 (2010) 153105.
[29] X. Li, W. Cai, L. Colombo, R.S. Ruoff, Evolution of graphene growth on Ni and Cu by carbon isotope labeling, Nano Lett. 9 (2009) 4268–4272.
[30] A.T.T. Koh, Y.M. Foong, D.H.C. Chua, Cooling rate and energy dependence of pulsed laser fabricated graphene on nickel at reduced temperature, Appl. Phys. Lett. 97 (2010) 114102.